EPTT 2024
Escola de Primavera de Transição e Turbulência

ABCM
Associação Brasileira de Engenharia e Ciências Mecânicas

EPTT-2024-0002
PRESSURE FIELD IN A CENTRIFUGAL PUMP COMPUTED FROM PARTICLE IMAGE VELOCIMETRY

Rafael F. L. Cerqueira[1‡]
William D. P. Fonseca[2]
Rodolfo M. Perissinotto[3]
William Monte Verde[3]
Erick M. Franklin[2]
Marcelo S. Castro[2,3]
[1]Mechanical Engineering Department, Federal University of Santa Catarina
[2]School of Mechanical Engineering, University of Campinas
[3]Center for Energy and Petroleum Studies, University of Campinas
[‡]rafael.cerqueira@ufsc.br

Abstract. *This paper presents an assessment study of the pressure field estimation from planar Particle Image Velocimetry (PIV) velocity fields. The method adopted to perform this task is based on the solution of Poisson equations for pressure, which are more adequate for complex geometries than the direct integration of pressure gradients. When dealing with Poisson equations, the application of boundary conditions is simpler, requiring only the implementation of a numerical method to solve the elliptic partial differential equation. For this class of PIV-based pressure estimator, some methods were proposed for the source term calculation in the past decades, including the modification of spatial derivative calculations, the inclusion of additional terms to account for out-of-plane velocities, and the filtering/smoothing of velocity fields. In this context, this work presents an study of different pressure Poisson-based estimator methodologies from PIV velocity measurements, including alternatives for the source term calculation and the effect of filtering/smoothing the instantaneous fields. These velocity fields are obtained using an experimental setup equipped with a time-resolved PIV system that perform measurements in a transparent centrifugal pump. Direct pressure measurements are also carried out in the pump prototype, using pressure transducers installed at different ports placed throughout the volute geometry. Thus, the pressure values from PIV fields are compared against the time-averaged values of the pressure measured by the sensors. Our results reveal that the PIV-based pressure estimator presents a satisfactory agreement with the transducer pressure values, being able to capture transient effects as well. The pressure fields in the pump also follow Computational Fluid Dynamics (CFD) results from the literature, which demonstrates that the PIV-based pressure solver can produce reliable results.*

Keywords: *Particle image velocimetry, pressure field, centrifugal pump.*

1. INTRODUCTION

Centrifugal pumps are widely used in a range of industrial applications. Due to its widespread use, particular interest was devoted to better understanding the flow structure within centrifugal pump equipment. Recently, due to the advances in experimental techniques, in special the Particle Image Velocimetry (PIV) technique, experimental studies focused on the internal flow structures have been performed (Pedersen *et al.*, 2003; Byskov *et al.*, 2003; Krause *et al.*, 2005; Keller *et al.*, 2014; Liu *et al.*, 2022; Chen *et al.*, 2022; Perissinotto *et al.*, 2023a,b; Fonseca *et al.*, 2023) . In certain situations, the pump may operate out of its design conditions, resulting in complex flow structures within the pump impellers and volute channels (Gülich, 2008).

In general, for single-phase flows, these studies focused on analyzing the velocity fields, instantaneous or average, by means of the PIV and Laser Doppler Velocimetry (LDV) techniques (Perissinotto *et al.*, 2021). These studies resulted in rich analyses of the internal flow structure, such as the intricate interaction between the pump impeller blades and the volute tongue (Keller *et al.*, 2014) and the alternating stall dynamics (Krause *et al.*, 2005; Liu *et al.*, 2022), a phenomenon that may occur during off-design operational conditions.

In certain cases, for instance when developing hydraulic loss models (Gülich, 2008) or mechanistic pump models (Zhu *et al.*, 2022) based on the PIV velocity results, the spatial pressure distributions within the centrifugal pump may help better understand the internal flow structure and also provide quantitative information. Prior to recent PIV technique advancements in laser, computer and camera technology (Raffel *et al.*, 1998), Gurka *et al.* (1999) estimated the pressure field distribution from the ensemble average 2D PIV velocity fields. Following this work, multiple authors derived numerical formulations to estimate the pressure fields from the PIV velocity files, such as Liu and Katz (2006), Murai *et al.* (2007), Charonko *et al.* (2010), De Kat and Van Oudheusden (2012), and Felis-Carrasco *et al.* (2021). The review article by Van Oudheusden (2013) presents an overview of the different numerical formulations and applications of PIV-based pressure solvers in different situations.

Following these lines, the current study presents the development of an instantaneous PIV-based pressure solver suitable for centrifugal pumps. As opposed to previous numerical implementations found in the literature, when working with centrifugal pumps, modifications are necessary to account for the rotational movement of the impeller blades. Thus, the numerical development of a PIV-based pressure solver is detailed here, presenting a numerical solver adequate for a broad range of internal and external flow applications, including rotating and translating boundaries, as in the case of the pump's impeller blades. Different pressure formulations are implemented in the numerical code. In order to assess the accuracy and robustness of the different pressure formulations, the pressure solver is tested against analytical solutions. Finally, the PIV-based pressure solver is applied to estimate the instantaneous pressure fields within a centrifugal pump prototype under different operational conditions.

2. EXPERIMENTAL SETUP

The experimental setup consists of a water line, a booster pump, a pump prototype, and instruments to measure the flow rate, pressure, and temperature. The flow rate is measured by a *Emerson MicroMotion F200* Coriolis flowmeter. The pressure is measured by *Emerson Rosemount 2051* capacitive transducers. The temperature is measured by a resistance sensor, PT100 type. The test section is essentially a transparent centrifugal pump, made of acrylic, and developed to enable flow visualization in the impeller and volute. Figure 1a) shows the transparent pump prototype mounted to the test section. The pump impeller has an inner and outer impeller radius of, respectively, R_{min} = 22 mm and R_{max} = 54.5 mm, while the channel height is h = 6 mm. The volute was designed following the guidelines from Stepanoff (1957) and Petermann and Pfleiderer (1964), resulting in volute minimum radius of $R_{vol,min}$ = 58.5 mm and maximum radius of $R_{vol,max}$ = 92.0 mm. Further details regarding the prototype construction can be found in Perissinotto *et al.* (2022).

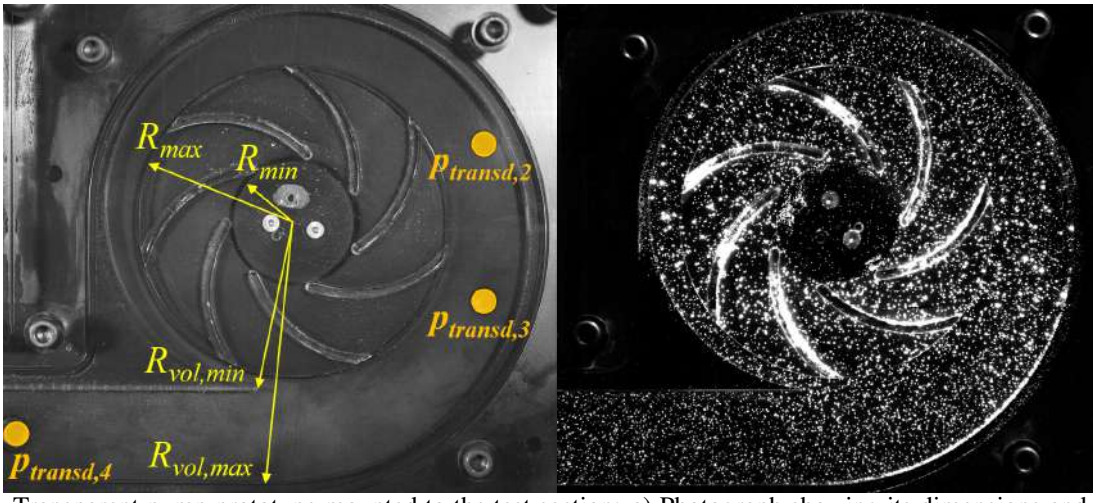

Figure 1: Transparent pump prototype mounted to the test section: a) Photograph showing its dimensions and positions of pressure ports; and b) Typical image acquired from the PIV system in the present work.

As Fig. 1a) suggests, the pump prototype has a total of four pressure measurement ports, three positioned on the volute channel and a fourth ($p_{\mathrm{transd},1}$) located before the inlet diffuser, that is not visible in the figure. The static pressure on these points is measured by differential pressure transducers calibrated to operate within a -0.5 bar to 1.5 bar range. During the differential pressure measurement, the reference values are taken from the pressure port located prior to the inlet diffuser, which we assumed as the pressure at the inlet of the impeller channels. During the PIV-based pressure measurement, described in the next paragraphs, the value of $p_{\mathrm{transd},1}$ and $p_{\mathrm{transd},4}$ are taken as boundary conditions, while the differential pressures $p_{2-1} = p_{\mathrm{transd},2} - p_{\mathrm{transd},1}$ and $p_{3-1} = p_{\mathrm{transd},3} - p_{\mathrm{transd},1}$ are adopted to assess the results of the PIV-based pressure Poisson's solver. Further details regarding the measurement port position and the pump prototype geometry can be found in Perissinotto *et al.* (2022).

The Time-Resolved PIV (TR-PIV) system is a *DualPower 30-1000* model provided by *Dantec Dynamics*. A *Phantom VEO640* high-speed camera, with a 2560 x 1600 pixel spatial resolution and 1400 fps temporal resolution, is used for PIV images acquisition. In order for the laser sheet to illuminate the entire transparent section, the laser beam coming from the laser source is divided into two beams. Then, a set of mirrors and lenses guide the beams towards the left and right edges of the test section, where another set of lenses creates the planar sheet. It is possible to completely illuminate the entire test section by illuminating the test section with two laser sheets. Figure 1b) shows a typical PIV image obtained through this illumination setting. In order to reduce reflections originating from the acrylic volute and impeller blades, fluorescent particles (average diameter of 50 μm) of PMMA doped with Rhodamine were used as tracers. In addition, as observed in Fig. 1a), the volute background and the impeller hub are made of black anodized aluminium to further avoid reflections. According to Fig.1b), the PIV images are uniformly illuminated without any shadows or reflections. Details regarding the PIV system setup are available in Perissinotto *et al.* (2023a).

3. EXPERIMENTAL MATRIX

The experimental matrix, comprised of 3 flow conditions, is shown in Tab. 1. It has a single pump rotational speed N and three different water flow rates Q_w. The water flow rate is also given in terms of the best efficiency point (BEP) of the transparent pump, Q_{BEP}, represented by the variable Q^*.

Table 1: Test matrix of the experiments performed in this work.

Experiment	N [rpm]	Q_w [m^3/h]	$Q^* = Q_w/Q_{BEP}$
1	600	0.45	0.3
2	600	1.50	1.0
3	600	2.20	1.5

For each experimental point, TR-PIV acquisitions were made with an acquisition frequency or temporal resolution of $f_{TR-PIV} = 700$ Hz. The velocity vectors were estimated using the *Adaptive PIV* analysis algorithm present in software *DynamicStudio 7.4* by *Dantec Dynamics*. We employed initial interrogation windows of 64x64 pixel and final interrogation windows of 32x32 pixel and 50% overlap. The images were acquired in a double-frame configuration, with a temporal spacing ΔT_{PIV} carefully chosen to limit the maximum displacement of the tracer particles to 8 pixels between two consecutive frames, following the guidelines discussed in Raffel *et al.* (1998).

Before computing the PIV velocity fields, an image rotation step must be added to the original PIV images to remove the solid body motion of the impeller blades (Liu *et al.*, 2021). Since the PIV acquisitions described here are related to the pump's volute and impeller channels, the domain was divided into two regions by a masking procedure. First, the PIV velocity fields in the impeller channels were estimated following the method described in Liu *et al.* (2021). By using this technique, the PIV velocity fields are computed in the impeller according to a non-inertial frame of reference due to the impeller blade movement correction, i.e., the velocity fields rotate together with the pump impeller. Then, more velocity vectors are calculated in the volute, without any image manipulation, since this spatial domain is intrinsically stationary. The PIV fields of the impeller and volute are finally merged into a single velocity field. During this step, the impeller velocity field is returned to its inertial frame of reference by adding the circumferential velocity field $\mathbf{U}_{\mathrm{circ}} = \omega \times \mathbf{r}$, in which ω is the angular speed and $\mathbf{r}$ is the distance vector from the impeller center. The entire procedure adopted in the present manuscript is carefully described in Perissinotto *et al.* (2023a).

4. PRESSURE FIELD ESTIMATION

The pressure field estimation performed in this paper depends on numerical implementations of mathematical expressions based on Poisson equations. The next sections present a description on the procedure developed for the calculations.

4.1 Background

This section provides a short outline of the general expressions used to determine the instantaneous pressure. Under incompressible flow assumptions, the Navier-Stokes equations read as:

$$\rho \frac{\mathrm{D}\mathbf{u}}{\mathrm{D}t} = -\nabla p + \mu \nabla^2 \mathbf{u}, \tag{1}$$

in which $\mathbf{u}$ is the instantaneous velocity vector, p is the pressure, ρ is the water density, and μ is its viscosity. The term $\mathrm{D}\mathbf{u}/\mathrm{D}t$ represents the material acceleration, which can be expressed in a Eulerian reference as:

$$\frac{\mathrm{D}\mathbf{u}}{\mathrm{D}t} = \frac{\partial \mathbf{u}}{\partial t} + (\mathbf{u}\cdot\nabla)\mathbf{u}. \tag{2}$$

Since the $\mathbf{u}$ velocity vector field is computed via the PIV measurement technique, by rearranging the Navier-Stokes equation, we can simply compute the pressure as:

$$\nabla p = -\rho\left[\frac{\partial \mathbf{u}}{\partial t} + (\mathbf{u}\cdot\nabla)\mathbf{u}\right] + \mu\nabla^2\mathbf{u}. \tag{3}$$

If the velocity field is measured by a two-dimensional planar PIV system, the expression above results in two equations for pressure gradient, one equation for $\partial P/\partial x$ and a second for $\partial P/\partial y$. The planar flow assumption, despite being strong, has demonstrated to provide reliable results in a range of applications, as listed and detailed in the review paper of Van Oudheusden (2013).

By specifying a set of adequate boundary conditions, the pressure field can be estimated by a direct integration method through a spatial marching procedure. For simple geometries, such as rectangular domains, the application of the technique is straightforward. However, this is not a feasible option in the present paper, since the pump geometry is complex and the impeller blades rotate during the experiment, a condition that makes the marching approach more difficult.

Due to the aforementioned reasons, in the present manuscript we opted to use the Poisson equation for the pressure (Van Oudheusden, 2013). This approach was also adopted in Gurka *et al.* (1999) to estimate the pressure field in laminar pipe flow with a constriction and an impinging air jet. Murai *et al.* (2007) employed the same Poisson-based approach for computing the pressure field around a turbine. The Poisson equation is derived by taking the divergence of Eq. (3):

$$\nabla^2 p = \nabla\cdot\left\{-\rho\left[\frac{\partial \mathbf{u}}{\partial t} + (\mathbf{u}\cdot\nabla)\mathbf{u}\right] + \mu\nabla^2\mathbf{u}\right\}. \tag{4}$$

By applying the incompressible form of the continuity equation, $\nabla\cdot\mathbf{u} = 0$, the Poisson equation reduces to:

$$\nabla^2 p = -\rho\nabla\cdot(\mathbf{u}\cdot\nabla)\mathbf{u}, \tag{5}$$

in which the unsteady and viscous term disappear. However, as pointed out by Van Oudheusden (2013), this property does not necessarily imply that the pressure field can be obtained from the instantaneous velocity fields alone, since time-dependent information can still be prescribed by the boundary conditions. In a 2D Cartesian coordinate system, the Poisson equation for pressure reads:

$$\frac{\partial^2 p}{\partial x^2} + \frac{\partial^2 p}{\partial y^2} = -\rho\left\{\left(\frac{\partial u}{\partial x}\right)^2 + 2\frac{\partial v}{\partial x}\frac{\partial u}{\partial y} + \left(\frac{\partial v}{\partial y}\right)^2\right\}. \tag{6}$$

Alternatively, by invoking the incompressible form of the continuity equation, we can also write (Murai *et al.*, 2007):

$$\frac{\partial^2 p}{\partial x^2} + \frac{\partial^2 p}{\partial y^2} = -2\left(\frac{\partial v}{\partial x}\frac{\partial u}{\partial y} - \frac{\partial u}{\partial x}\frac{\partial v}{\partial y}\right). \tag{7}$$

Despite Eqs. (6) and (7) being equivalent in theory, the numerical implementation of the equations can dramatically alter the pressure estimation. For this reason, the following nomenclature is used in the following paragraphs: Eq. (6) is referred as '*Poisson-1*', while Eq. (7) is referred as '*Poisson-2*'. When using the pressure Poisson equation to estimate the pressure field from the PIV values, appropriated boundary conditions must be supplied, such as Dirichilet condition for a known pressure or a Neumann form using Eq. (3).

4.2 Numerical implementation

The pressure field is estimated by numerically solving the discretized versions of Eqs. (6) and (7). In the present work, the pressure terms, LHS of Eqs. (6) and (7), are discretized using second-order central finite differences. Similarly, the spatial derivatives on the RHS of both equations are also computed using second-order central finite differences. However, as opposed to the pressure terms, the RHS terms are calculated from the PIV values and can be interpreted as explicit source terms. The discretized pressure Poisson equation takes form:

$$\frac{p_W - p_P + p_E}{\Delta x^2} + \frac{p_N - p_P + p_S}{\Delta y^2} = S_{\mathrm{PIV}}, \tag{8}$$

where the subscript in $p_{\{W,E,N,S\}}$ denotes the neighbor position on a 5 point stencil grid, as illustrated in Fig. 2. The S_{PIV} term on the RHS of Eq. (8) represents the PIV velocity related terms, which are defined by '*Poisson-1*' and '*Poisson-2*' formulations. After discretizing the equations and applying the boundary conditions, Eq. (8) can be assembled into a pentadiagonal linear system to estimate the pressure in each PIV interrogation window. The system of equations reads:

$$[\boldsymbol{A}]_{(N_x \cdot N_y)\times(N_x \cdot N_y)}\,[\boldsymbol{p}]_{(N_x \cdot N_y)\times 1} = [\boldsymbol{B}]_{(N_x \cdot N_y)\times 1}\,, \tag{9}$$

where $[\boldsymbol{A}]$ is a the pentadiagonal coefficient matrix, $[\boldsymbol{p}]$ is the solution vector, and $[\boldsymbol{B}]$ is the RHS vector. The N_x refers to the number of PIV interrogation windows in the x direction, while N_y for the y direction. The matrix is assembled using Python's scipy package (Virtanen *et al.*, 2020) with the Compressed Sparse Row (CSR) format and solved with `scipy.sparse.linalg.gmres` Generalized Minimal RESidual iteration (GMRES) solver.

Equation (8) is implemented in an in-house Python code that reads the PIV velocity field, assigns the appropriate boundary conditions, assemble and solves the linear system of equations, hence, estimating the pressure field from the PIV velocity fields. The implementation was developed aiming its use with complex internal and external geometries, as in the case with the centrifugal pump studied here. Thus, following the structured Cartesian nature of the PIV velocity fields, a staircase approximation is applied to approximate the curved boundaries of the volute wall and impeller blades. Figure 2 presents a schematic representation of the adopted approach and details of the element numbering and connectivity.

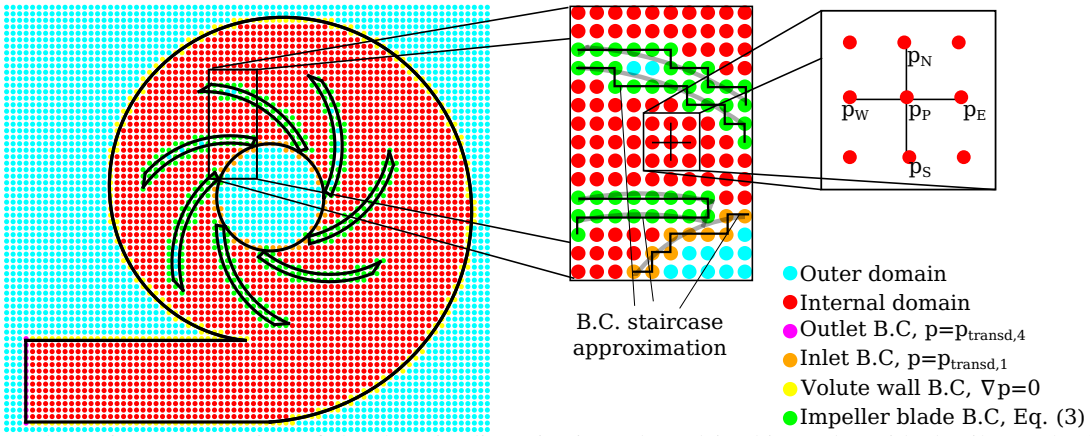

Figure 2: Schematic representation of the domain discretization adopted in this study, with details on the boundary condition definition and the index connectivity used to assemble the coefficient matrix.

As noticed from Fig. 2, a Cartesian structured mesh, with equidistant nodes, is used to discretize the domain. However, to simplify the numerical implementation, some nodes are defined as 'outer nodes', which are not used when assembling the coefficient matrix, while others are treated as internal or B.C. nodes. The domain discretization and boundary condition definition adopted here were developed to be as general as possible, such that the use of a rotating or translating geometry is straightforward. That is the case in the present work, where the impeller blade rotates around its center, and the boundary conditions rotate accordingly.

5. RESULTS AND DISCUSSIONS

The following sections report the main results obtained from the pressure field estimation, including the tool validation using an analytical solution and the tool utilisation using real experimental data.

5.1 Verification and Validation

Following the study of Charonko *et al.* (2010), the entire numerical implementation was tested against a model flow field with exact analytical solutions for pressure and velocity. In the present work, the implementation results were tested with a decaying Taylor vortex flow centered at the domain center:

$$u_\theta(r,t) = \frac{A}{8\pi}\frac{r\rho}{\mu t^2}\exp\left(-\frac{\rho r^2}{4\mu t}\right), \tag{10}$$

where $u_\theta(r,t)$ is the tangential velocity in a position r away from the domain center at time t, and A is a measure of the angular momentum in the vortex (Charonko *et al.*, 2010). Using the Navier-Stokes equations in cylindrical coordinates and solving for the pressure:

$$p(r,t) = \frac{\rho^2 A^2}{64\pi^2 \nu t^3}\left[-\exp\left(-\frac{\rho r^2}{2\mu t}\right)\right] + P_\infty, \tag{11}$$

where P_∞ is the pressure at a infinite distance from the origin, here set as P_∞ = 0.0 Pa. For the numerical implementation verification against the decaying Taylor vortex flow, the value of vortex momentum was set to $A = 1.0 \times 10^{-6}$ m², and the numerical domain was defined as a square with sides $L = H = 1.0 \times 10^{-3}$ m. The numerical grid was set to $N_x = N_y =$ 51 points and a total of t_f = 3.0 s were simulated using a Δt = 0.03 s time step.

Again, following Charonko *et al.* (2010), in order to mimic the associated uncertainties of the PIV technique, the values from the synthetic fields from Eq. (11) were modified by a small amount of controlled random error. Thus, it was possible to analyze the robustness of the '*Poisson-1*' and '*Poisson-2*' formulations to cope with the inherent uncertainty associated with PIV velocity values, typical when using time-resolved PIV velocity fields, where no averaging is applied to smooth out high-frequency errors.

An alternative to alleviate the problems associated with PIV uncertainties when estimating the pressure is to apply a filtering or smoothing process to the instantaneous PIV velocity fields (Charonko *et al.*, 2010). In the present paper, this is accomplished by a smoothing filter based on Proper Orthogonal Decomposition (POD). It is worth mentioning that POD is a mode decomposition method used in fluid dynamics to decompose the flow field into a set of deterministic functions (Weiss, 2019). Here, the POD is used as a filter by decomposing the TR-PIV velocity fields and only retaining their most energetic modes, which are closely associated with the flow structure and not with the high-frequency uncertainties. When using a POD-based smoothing filter, it is necessary to define a threshold to remove the least energetic contributions. Charonko *et al.* (2010) set the smoothing threshold to discard modes that contributed less than 1% to the total energy. In the present paper, only the five first modes were used to reconstruct the velocity fields when applying the POD-based smoothing filter, by analysing the energy distribution within the modes.

Therefore, the PIV-based pressure estimator developed in the present work was tested in four different configurations, '*Poisson-1*' and '*Poisson-2*' with and without the POD-based smoothing filter. These tests were performed by varying the degree of the controlled random error and by calculating the root-mean-square (RMS) error relative to the analytical pressure solution from Eq. (11). The RMS error value was determined for each timestep, from $t = 0$ to $t = t_f$, representing the total deviation from the analytical pressure field during an entire test run. As an illustrative example, Fig. 3 shows a snapshot of both the velocity and pressure fields at a given instant of time, revealing the analytical results and also the error-contaminated fields at a given numerical configuration.

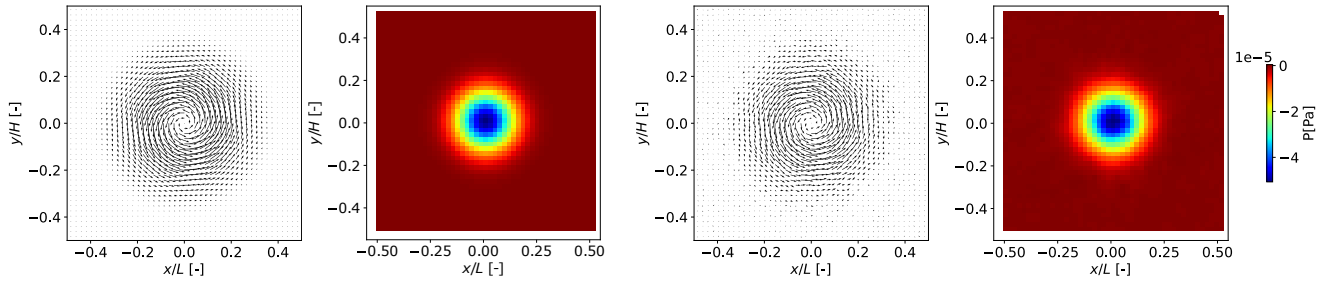

Figure 3: Example of the velocity and pressure fields from the decaying Taylor vortex flow: a) Uncorrupted velocity fields and b) Velocity fields with an imposed error of 10%. The numerical results corresponds to the '*Poisson-2*' configuration, without POD-based filtering, and at t = 0.3 s.

Figure 4 displays the RMS error against different levels of imposed random contributions for the four tested pressure estimator configurations. According to the figure, the '*Poisson-2*' pressure formulation presents the best results and it is more noise tolerant than the '*Poisson-1*' pressure formulation. Regarding the POD-smoothing, the results from Fig. 4b) indicate that its application provides a lower RMS error, presenting almost constant error values for the different imposed random noise perturbations. In addition, the same trend shown in Fig. 4a) for the '*Poisson-1*' is also observed in the work of Charonko *et al.* (2010).

Figure 5 shows the estimated pressure field with an imposed error level of 5.0% in the two tested configurations with POD-based smoothing filter and the reference value computed from Eq. (11). By comparing the estimated pressure fields from the POD-based formulations in Fig. 5, it is clear that the '*Poisson-1*' option is not able to reconstruct the pressure field, as opposed to the results from the '*Poisson-2*' formulation.

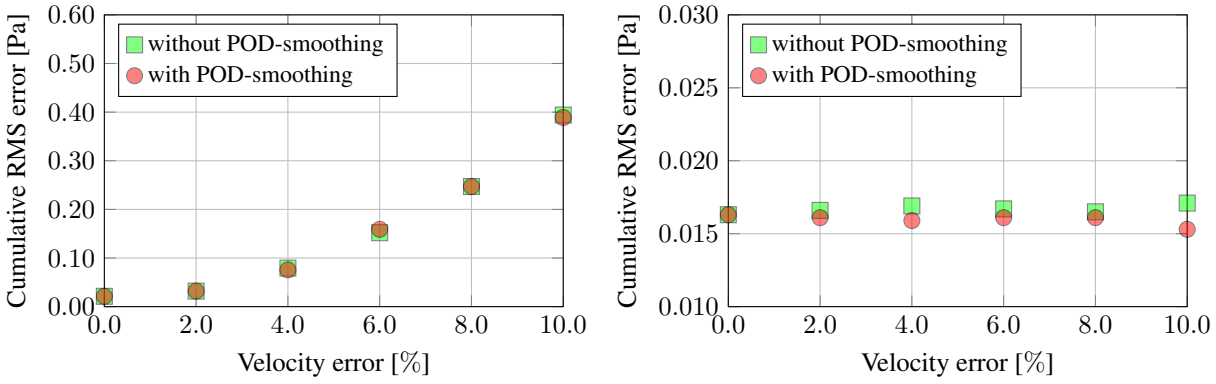

(a) '*Poisson-1*' - Eq. (6) (b) '*Poisson-2*' - Eq. (7)

Figure 4: Numerical assessment of '*Poisson-1*' and '*Poisson-2*' pressure formulations with and without POD-based filter.

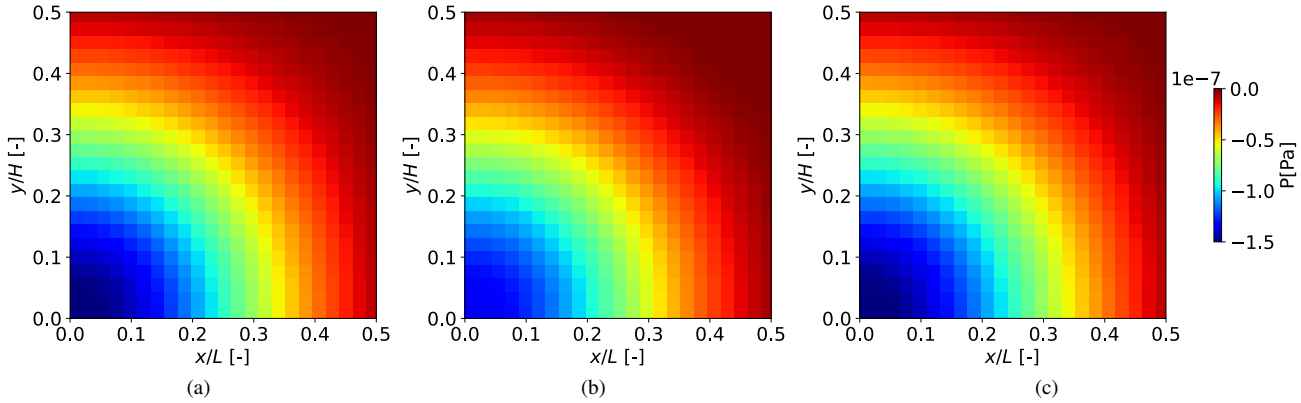

(a) (b) (c)

Figure 5: Estimated pressure fields from the synthetic PIV fields from the decaying Taylor vortex flow at $t = 2.1$ s for different pressure formulations with an imposed error level of 5.0 %: a) Reference field - Eq. (11); b) '*Poisson-1*' - with POD-based filtering and c) '*Poisson-2*' - with POD-based filtering. Only a quarter of the domain is plotted here.

Therefore, based on the results depicted in Figs. 4 and 5, the '*Poisson-2*' formulation with the POD-based smoothing filter is selected as the most appropriate approach to estimate the pressure field within the centrifugal pump using the transient PIV velocity fields. This is done in the next section.

5.2 PIV-based pressure fields

In order to present the capabilities of our PIV-based pressure solver, Fig. 6 reveals the instantaneous pressure distribution within the centrifugal pump impeller and volute estimated by the solver described here for the different experiments listed in Tab. 1. The results from Fig. 6 were extracted at a given instant of the transient PIV results so that the impeller position is the same in the three cases. Details regarding the transient pressure evolution are described in the next paragraphs. When estimating the pressure field from the PIV results, the pressure at the impeller entrance (inlet) was defined as $p = 0$ kPa, while the pressure at the volute exit (outlet) was set as a constant value, measured from the differential pressure transducer, $p = 6.5$ kPa (Exp. 1), $p = 5.5$ kPa (Exp. 2) and $p = 0.5$ kPa (Exp. 3), where the gauge pressure values are zero-referenced to the ambient air pressure. According to Fig. 6, in the three configurations, a pressure gain is observed in the impeller channels. Although the pump prototype stage analyzed in the present work has a volute-type diffuser, the pressure gain within the different channels is homogeneous.

Analyzing the results from Fig. 6 at the volute geometry, it is possible to observe that the pump operational conditions have a significant impact on the pressure fields. For the Q^* = 0.3 experiment (Fig. 6a), there is a gradual increase of the pressure values throughout the volute geometry, reaching a maximum value at the pump outlet section. At the BEP condition (Fig. 6b), the pressure field distribution within the volute is more uniform when compared to the Q^* = 0.3 condition. Here, according to the PIV-based pressure fields, the pump volute is acting towards increasing the pressure energy of the flow since a pressure gain is observed when analyzing its distribution from the volute geometry's starting point until the pump outlet section. For the open-flow condition, Q^* = 1.5 experiment (Fig. 6c), the pressure distribution is uniform until the first half of the volute geometry. A pressure gain is observed from the second half of the geometry until the volute tongue. However, from the volute tongue on, the pressure decreases until the pump outlet section. According

to Keller *et al.* (2014), the flow close to the volute tongue is characterized by strong interactions between the tongue and the the tips of the impeller blades, which results in high turbulent intensities in the region. Therefore, higher energy dissipation is expected in this area, which explains the pressure energy loss from this region until the outlet section.

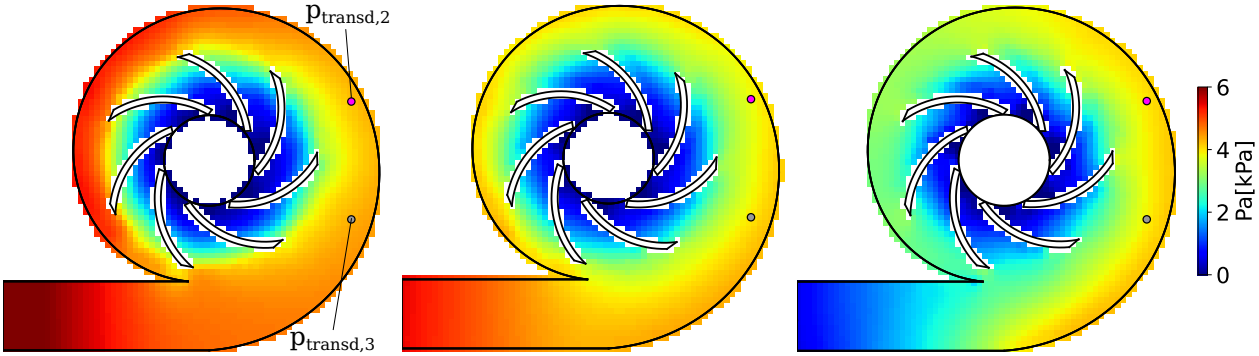

(a) N = 600 rpm and Q^* = 0.3 (b) N = 600 rpm and Q^* = 1.0 (c) N = 600 rpm and Q^* = 1.5

Figure 6: Instantaneous pressure fields within the centrifugal pump stage estimated from the PIV velocity fields for the experimental conditions listed in Tab. 1.

The pressure field distribution shown in Fig. 6 and described in the paragraphs above follow other results found in the literature for CFD simulations, such as the pressure distributions reported in Yuan *et al.* (2019) and Qu *et al.* (2016), which present the pressure distribution throughout the entire pump geometry at the shut-off, BEP, and open-flow conditions.

Despite the accordance of the PIV-based pressure fields with CFD results found in the literature, the results of the solver developed here could be compared against measurements from the two pressure points $p_{\text{transd},2}$ and $p_{\text{transd},3}$ located at the volute, as displayed in Figs. 1 and 6. Figure 7 contains the transient pressure values at $p_{\text{transd},2}$ and $p_{\text{transd},3}$ from the PIV-based pressure solver (calculation) and the differential pressure transducers (measurement). Since the data acquisition system installed at the experimental setup does not have a high temporal resolution, only the average values at these two positions are plotted for comparison.

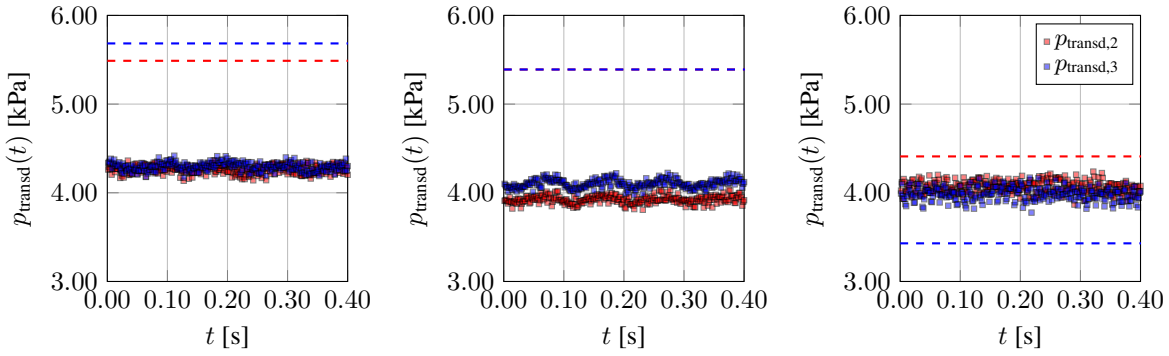

(a) N = 600 rpm and Q^* = 0.3 (b) N = 600 rpm and Q^* = 1.0 (c) N = 600 rpm and Q^* = 1.5

Figure 7: Instantaneous pressure values extracted from points $p_{\text{transd},2}$ and $p_{\text{transd},3}$ from the PIV-based pressure field and from the pressure transducers installed in the test section (see Figs. 1 and 6.) Dashed lines represent the pressure transducer values (experimental measurements), while points represent the PIV-based pressure transient values (calculations).

As shown in Fig. 7, the values from the differential pressure transducer and the ones from the PIV-based solver do not present a perfect agreement in the three different cases. Nevertheless, considering the experimental uncertainty related to the pressure transducers and the PIV acquisitions, we can conclude that the pressure estimation results in a satisfactory agreement. In special, the estimated PIV-based pressure solver follows the trend noted in the pressure transducer values, where $p_{\text{transd},3} > p_{\text{transd},2}$ in Exp. 1 and $p_{\text{transd},3} < p_{\text{transd},2}$ in Exp. 3.

The results from Fig. 7 also show that the PIV-based pressure solver can capture transient effects. In the three analyzed cases, the pressure values have presented a periodic pattern, with a characteristic period of approximately 0.1s, which matches the characteristic impeller frequency (600 rpm = 10 Hz). By analyzing the three transient pressure plots, we can observe that the periodic pattern is stronger at the BEP condition,Fig. 7b). This observation may indicate the passage of well-defined coherent structures flowing in the region close to the points where the pressure transducers are fixed.

6. CONCLUSIONS

The present work describes the development and assessment of an instantaneous PIV-based pressure solver suitable for time-resolved PIV acquisition within centrifugal pumps, where a set of dynamic boundary conditions are required due to the rotational impeller domain. Different numerical implementations based on the pressure Poisson equation found in the literature were tested in the present paper and validated against analytical results. The assessment study was based on the superposition of controlled random error velocity fields on top of the original velocity field, mimicking the inherent uncertainties associated with the PIV technique. In addition to different pressure Poisson formulations, the effect of POD filtering was tested on the final PIV-based pressure estimation following studies found in the literature. According to the analytical assessment study, the pressure Poison discretization proposed by Murai *et al.* (2007) with a POD-based filter resulted in low RMS errors even in situations with a large imposed velocity error.

In order to assess the PIV-based pressure solver developed and described in the current work, pressure fields estimated from time-resolved PIV acquisitions in a centrifugal pump under three different operational conditions were compared against experimental pressure measurements made by pressure transducers placed at two different points located at the pump's volute channel. The pressure values present an acceptable agreement, with the pressure-based fields capturing the overall trend of the pressure values along the volute channel, including transient effects from the periodic passage of the impeller blades. In addition, the pressure field from the PIV-based pressure solver follows results found in the literature for centrifugal pumps with similar geometry (Yuan *et al.*, 2019; Qu *et al.*, 2016). The results were satisfactory for the three flow rates analyzed in the test matrix, comprising design and off-design conditions.

From the assessment studies performed in the present work, it is possible to conclude that the PIV-based pressure solver detailed here is able to properly estimate the pressure field within a centrifugal pump stage. Therefore, the present methodology, capable of estimating pressure fields from time-resolved PIV results, may help improve the understanding on the energy losses in centrifugal pumps and even allow the development of more efficient pump performance models.

7. ACKNOWLEDGEMENTS

We gratefully acknowledge the support of EPIC - Energy Production Innovation Center, hosted by the University of Campinas (UNICAMP) and sponsored by FAPESP – The São Paulo Research Foundation (Process Number 2017/15736-3). We also thank FAPESP for providing the PIV system used in this research through the Multi-User Equipment program (Process Number 2019/20870-6). We acknowledge the support of ANP (Brazil's National Oil, Natural Gas and Biofuels Agency) through the R&D levy regulation. The acknowledgments are also extended to Center for Energy and Petroleum Studies (CEPETRO), School of Mechanical Engineering (FEM), and ALFA Research Group.

8. REFERENCES

Byskov, R.K., Jacobsen, C.B. and Pedersen, N., 2003. "Flow in a centrifugal pump impeller at design and off-design conditions—part ii: large eddy simulations". *J. Fluids Eng.*, Vol. 125, No. 1, pp. 73–83.

Charonko, J.J., King, C.V., Smith, B.L. and Vlachos, P.P., 2010. "Assessment of pressure field calculations from particle image velocimetry measurements". *Measurement Science and Technology*, Vol. 21. ISSN 13616501.

Chen, B., Li, X. and Zhu, Z., 2022. "Investigations of energy distribution and loss characterization in a centrifugal impeller through piv experiment". *Ocean Engineering*, Vol. 247, p. 110773.

De Kat, R. and Van Oudheusden, B.W., 2012. "Instantaneous planar pressure determination from PIV in turbulent flow". *Experiments in Fluids*, Vol. 52, No. 5, pp. 1089–1106. ISSN 07234864.

Felis-Carrasco, F., Watz, B.B., Hess, D. and Mendez, M.A., 2021. "A study on PIV-based pressure measurements using CFD techniques". *14th International Symposium on Particle Image Velocimetry – ISPIV 2021*.

Fonseca, W.D., Cerqueira, R.F., Perissinotto, R.M., Verde, W.M., Castro, M.S. and Franklin, E.M., 2023. "Particle image velocimetry in the impeller of a centrifugal pump: A pod-based analysis". *Flow Measurement and Instrumentation*, Vol. 94, p. 102483.

Gülich, J.F., 2008. *Centrifugal pumps*, Vol. 2. Springer.

Gurka, R., Liberzon, A., Hefetz, D., Rubinstein, D. and Shavit, U., 1999. "Computation of pressure distribution using piv velocity data". In *Workshop on particle image velocimetry*. Vol. 2, pp. 1–6.

Keller, J., Blanco, E., Barrio, R. and Parrondo, J., 2014. "Piv measurements of the unsteady flow structures in a volute centrifugal pump at a high flow rate". *Experiments in Fluids*, Vol. 10, No. 55, pp. 1–14.

Krause, N., Zähringer, K. and Pap, E., 2005. "Time-resolved particle imaging velocimetry for the investigation of rotating stall in a radial pump". *Experiments in Fluids*, Vol. 39, No. 2, pp. 192–201.

Liu, X.D., Li, Y.J., Liu, Z.Q. and Yang, W., 2022. "Dynamic stall inception and evolution process measured by high-frequency particle image velocimetry system in low specific speed impeller". *Journal of Fluids Engineering*, Vol. 144, No. 4, p. 041504.

Liu, X.D., Liu, Z.Q., Zhong, Q., Li, Y.j. and Yang, W., 2021. "Experimental investigation of relative velocity field based

on image rotation method in pump impeller". *Flow Measurement and Instrumentation*, Vol. 82, p. 102061.

Liu, X. and Katz, J., 2006. "Instantaneous pressure and material acceleration measurements using a four-exposure PIV system". In *Experiments in Fluids*. Vol. 41, pp. 227–240. ISSN 07234864.

Murai, Y., Nakada, T., Suzuki, T. and Yamamoto, F., 2007. "Particle tracking velocimetry applied to estimate the pressure field around a Savonius turbine". *Measurement Science and Technology*, Vol. 18, No. 8, pp. 2491–2503. ISSN 13616501.

Pedersen, N., Larsen, P.S. and Jacobsen, C.B., 2003. "Flow in a centrifugal pump impeller at design and off-design conditions—part i: particle image velocimetry (piv) and laser doppler velocimetry (ldv) measurements". *J. Fluids Eng.*, Vol. 125, No. 1, pp. 61–72.

Perissinotto, R., de Cerqueira, R.F.L., Fonseca, W.D.P., Verde, W.M., Biazussi, J.L., de Moraes Franklin, E., de Castro, M.S. and Bannwart, A., 2022. "Development of a transparent pump prototype for flow visualization purposes". *Rio Oil & Gas*.

Perissinotto, R.M., Cerqueira, R.F., Fonseca, W.D., Verde, W.M., Biazussi, J.L., Bannwart, A.C., Franklin, E.M. and Castro, M.S., 2023a. "Particle image velocimetry in a centrifugal pump: Details of the fluid flow at different operation conditions". *Flow Measurement and Instrumentation*, Vol. 89, p. 102282.

Perissinotto, R.M., Fonseca, W.D., Cerqueira, R.F., Verde, W.M., Bannwart, A.C., Franklin, E.M. and Castro, M.S., 2023b. "Particle image velocimetry in a centrifugal pump: Influence of walls on the flow at different axial positions". *Journal of Fluids Engineering*, pp. FE–23–1301.

Perissinotto, R.M., Verde, W.M., Biazussi, J.L., Bulgarelli, N.A.V., Fonseca, W.D.P., de Castro, M.S., de Moraes Franklin, E. and Bannwart, A.C., 2021. "Flow visualization in centrifugal pumps: A review of methods and experimental studies". *Journal of Petroleum Science and Engineering*, Vol. 203, p. 108582.

Petermann, H. and Pfleiderer, C., 1964. *Strömungsmaschinen*. Springer.

Qu, W., Shuliang, C., Wang, Y., Xu, Y. *et al.*, 2016. "Numerical investigation of clocking effect on a centrifugal pump with inlet guide vanes". *Engineering Computations*.

Raffel, M., Willert, C.E., Kompenhans, J. *et al.*, 1998. *Particle image velocimetry: a practical guide*, Vol. 2. Springer.

Stepanoff, A.J., 1957. "Centrifugal and axial flow pumps". *Theory, Design, and Application*.

Van Oudheusden, B.W., 2013. "PIV-based pressure measurement". *Measurement Science and Technology*, Vol. 24, No. 3. ISSN 13616501.

Virtanen, P., Gommers, R., Oliphant, T.E., Haberland, M., Reddy, T., Cournapeau, D., Burovski, E., Peterson, P., Weckesser, W., Bright, J., van der Walt, S.J., Brett, M., Wilson, J., Millman, K.J., Mayorov, N., Nelson, A.R.J., Jones, E., Kern, R., Larson, E., Carey, C.J., Polat, İ., Feng, Y., Moore, E.W., VanderPlas, J., Laxalde, D., Perktold, J., Cimrman, R., Henriksen, I., Quintero, E.A., Harris, C.R., Archibald, A.M., Ribeiro, A.H., Pedregosa, F., van Mulbregt, P. and SciPy 1.0 Contributors, 2020. "SciPy 1.0: Fundamental Algorithms for Scientific Computing in Python". *Nature Methods*, Vol. 17, pp. 261–272.

Weiss, J., 2019. "A tutorial on the proper orthogonal decomposition". In *AIAA Aviation 2019 Forum*. p. 3333.

Yuan, Y., Yuan, S. and Tang, L., 2019. "Numerical investigation on the mechanism of double-volute balancing radial hydraulic force on the centrifugal pump". *Processes*, Vol. 7, No. 10, p. 689.

Zhu, H., Zhu, J. and Zhang, H.Q., 2022. "Mechanistic modeling of gas effect on multi-stage electrical submersible pump (esp) performance with experimental validation". *Chemical Engineering Science*, Vol. 252, p. 117288.

9. RESPONSIBILITY NOTICE

The authors are the only responsible for the printed material included in this paper.